Enhanced encephalitic tropism of bovine H5N1 compared to the Vietnam H5N1 isolate in mice

Kerry Goldin[1#], Sarah van Tol[1#], Randall C. Johnson[3], Reshma Koolaparambil Mukesh[1], Shane Gallogly[1], Jonathan E. Schulz[1], Jessica Prado-Smith[2], Greg Saturday[2], Kwe Claude Yinda[1], Vincent J. Munster[1], Emmie de Wit[1], Neeltje van Doremalen[1*]

1. Laboratory of Virology, National Institute of Allergy and Infectious Diseases, National Institutes of Health, Hamilton, MT, USA
2. Rocky Mountain Veterinary Branch, National Institute of Allergy and Infectious Diseases, National Institutes of Health, Hamilton, MT, USA
3. Integrated Data Science Section, Research Technology Branch, National Institute of Allergy and Infectious Diseases, National Institutes of Health, MD, USA

#These authors contributed equally

*Corresponding author: Neeltje van Doremalen, 903 south 4th street, Hamilton, MT, USA. neeltje.vandoremalen@nih.gov

Author contributions: NvD designed the study; KG, SvT, RCJ, RKM, SG, JES, GS, KCY, VJM, EdW, and NvD acquired, analyzed, and interpreted the data; KG, SvT, and NvD wrote the manuscript. All authors have approved the submitted version.

COI statement: The authors declare no conflict of interest.

Keywords: Influenza A virus, avian influenza virus, H5N1, mouse, aerosols, challenge model, animal model, CNS, tropism

This PDF file includes:

Main Text

Figures 1 to 4

Abstract:

In recent years, the landscape of highly pathogenic avian influenza (HPAI) virus infections has shifted, as evidenced by an increase in infections among mammals. This includes the recent circulation of H5N1 in dairy cattle herds in the USA and a rise in associated human cases. In this study, we investigated differences in tissue tropism of two HPAI H5N1 strains, the isolate A/Vietnam/1203/2004 (VN1203) isolated from a fatal human case in 2004 and the bovine isolate A/Bovine/Ohio/B24osu-342/2024 (Bov342) isolated in 2024, in C57BL/6J mice. Infection with either HPAI H5N1 isolate was uniformly lethal in mice. However, tissue tropism differed significantly: while VN1203 replication was largely restricted to the respiratory tract, Bov342 successfully replicated in the respiratory tract as well as various regions of the brain. Bov342-challenged animals exhibited clinical signs consistent with central nervous system (CNS) infection, and infectious virus was detected in brain tissue. Correspondingly, cytokine profiles in the brain differed significantly between the isolates. Notably, in addition to abundant evidence of CNS infection in Bov342-challenged mice via immunohistochemistry, sporadic intranuclear and intracytoplasmic immunoreactivity was observed in other tissues in the head, including the choroid plexus, retina, and inner ear. This study demonstrates that while both HPAI H5N1 isolates are uniformly lethal in C57BL/6J mice upon aerosol exposure, significant differences exist in tissue tropism, with Bov342 resulting in respiratory disease as well as increased neurotropism and inflammation in the brain and nasal turbinates compared to VN1203, which predominantly induces respiratory disease.

Significance statement:

The rise in HPAI H5N1 infections among mammals, including humans in the USA, highlights an emerging One Health concern. Understanding the phenotypic changes of HPAI H5N1 and associated increase in infection of mammalian hosts is critical. In this study, we investigated the tissue tropism in mice of a bovine HPAI H5N1 strain isolated in 2024 and compared it to a strain isolated from a human patient in 2004. Our findings reveal that the bovine isolate exhibits enhanced neurotropism, unlike the respiratory-restricted replication observed with the HPAI H5N1 isolate from 2004. This difference in

62 tissue tropism, accompanied by distinct cytokine responses in the brain, underscores the potential for

63 altered disease outcomes in other mammalian hosts.

Introduction

Recent years have seen an increase in spillover events where HPAI H5N1 viruses of clade 2.3.4.4b have crossed into a wide variety of species, including sea lions, mink, foxes, skunks, raccoons, and bobcats (1-3), which raises substantial concerns regarding the pandemic and panzootic potential of clade 2.3.4.4b HPAI H5N1 viruses. The increasing incidence of HPAI H5N1 virus in mammals underscores the urgent need for continued surveillance and research to better understand and mitigate the risk of a pandemic.

The first human case of HPAI H5N1 influenza virus infection was detected in 1997 in Hong Kong (4). Subsequently, HPAI H5N1 viruses rapidly diversified through reassortment with avian influenza viruses, leading to the emergence of a new genotype in clade 1: Z. Genotype Z spread throughout poultry in Southern China and was the only genotype detected by 2004 (5). Infection of poultry with genotype Z was also reported in China, Japan, South Korea, Thailand, Vietnam, Indonesia, Cambodia, and Laos (6). Human H5N1 infections were laboratory-confirmed in Vietnam, Cambodia, Indonesia, and Thailand, including fatal cases in Vietnam and Thailand (7, 8).

HPAI H5N1 (clade 2.3.4.4) was first detected in the United States and Canada in 2014 (6). A subclade, 2.3.4.4b, has displayed explosive expansion in wild birds (9) and was associated with fatal infections in mammals (1, 2, 10). Following reports of an abrupt drop in milk production and reduced feed intake by dairy cows in Texas and Kansas, milk and tissue samples from cattle tested positive for HPAI H5N1 by the Iowa State University Veterinary Diagnostic Laboratory (11). As of October 22, 2024, H5N1 has been reported in 492 herds across 15 states (12). Additionally, 25 human cases have been reported following exposure to dairy cows (13). A recent serologic survey across dairy workers demonstrated 7% (8 out of 115 persons) had evidence of a recent infection with H5N1 (14). One additional hospitalized case has not been associated with exposure to dairy cows or poultry, even though phylogenetic analysis shows clustering with bovine H5N1 isolates (15). All but one H5N1 human cases in the USA have been mild, resulting in conjunctivitis or respiratory symptoms (13).

In this study, we investigate whether the extensive evolution of HPAI H5N1 from genotype Z to the recent bovine HPAI H5N1 isolate results in differences in tissue tropism. We exposed C57BL/6J mice to

either bovine H5N1 (A/Bovine/Ohio/B24osu-342/2024, Bov342) or HPAI H5N1 isolate obtained from the upper respiratory tract of a human case in Vietnam in 2004 (A/Vietnam/1203/2004 (VN1203), genotype Z) (16). Exposure to virus was done via aerosols, to mimic a more natural route of infection. We chose VN1203 as a comparison, since it has been extensively studied by other groups in animal models (17-20). Upon exposure, mice in both groups displayed reduced activity and rapidly lost weight. Interestingly, whereas animals exposed to Bov342 showed neurological signs of disease, these signs were absent in animals exposed to VN1203. Accordingly, virus titers were high in brain tissue of Bov342-exposed animals compared to VN1203-exposed animals. Additionally, at endpoint cytokine levels were upregulated in brain tissue of Bov342-exposed animals, but not VN1203-exposed animals. Cytokine levels in lung tissues differed significantly between the isolates. Finally, immunohistochemistry showed markedly increased immunoreactivity in the brain, nasal turbinates and, to a lesser degree, the lungs in animals exposed to Bov342 compared to those exposed to VN1203. Thus, even though H5N1 exposure via aerosols is uniformly lethal for both VN1203 and Bov342 in C57BL/6J mice, tissue tropism differs, with Bov342 displaying a preference for the CNS and respiratory tract, whereas replication of VN1203 in the CNS is limited.

105 **Results**

106 *C57BL/6J mice display dose-dependent signs of disease after aerosol challenge with HPAI H5N1*

107 Mice were challenged with HPAI H5N1 A/Bovine/Ohio/B24osu-342/2024 (Bov342) or
108 A/Vietnam/1203/2004 (VN1203) via aerosols, resulting in an inhaled dose of approximately 10^2, 10^3, or
109 10^4 $TCID_{50}$ (**Figure 1a**). Activity levels of six animals per group were monitored continuously and totaled
110 per six hours. Compared to uninfected individuals, animals exposed to 10^4 $TCID_{50}$ Bov342 showed
111 reduced activity starting at 48 hours post exposure. Consistent reduced activity was delayed by a further
112 18 hours in the 10^3 dose group (66 hours post exposure) and 84 hours in the 10^2 dose group (132 hours
113 post exposure) compared to the 10^4 dose group. Reduced activity in the animals exposed to VN1203
114 compared to uninfected animals was observed at 54 hours and 102 hours post exposure in the 10^4 and 10^3
115 dose group respectively but was not consistently observed in the 10^2 dose group (**Figure 1b**). All six
116 groups displayed weight loss compared to uninfected controls, although this did not reach significance in
117 the 10^2 dose VN1203 group (**Figure 1c**). Endpoint criteria were reached in all six animals within the
118 Bov342 groups and 10^4 and 10^3 dose VN1203 groups, but two out of six animals did not reach endpoint
119 criteria in the 10^2 dose VN1203 group. Survival was dose-dependent; animals that received a lower dose
120 of virus reached endpoint criteria later than those that received the highest dose of virus (**Figure 1d**). One
121 of the two surviving animals was seronegative for neuraminidase (A/bald eagle/Florida/W22-134-
122 OP/2022) and HA (VN1203) at 28 days post exposure, and thus did not have a productive virus infection
123 (**Supplementary Figure 1a-b**). Clinical signs in mice differed depending on what virus isolate the
124 animals were inoculated with: animals inoculated with Bov342 displayed signs indicative of infection of
125 the central nervous system (CNS), including tremors and ataxia, whereas animals inoculated with
126 VN1203 displayed primarily respiratory signs, including a hunched posture and tachypnea to dyspnea.
127 Oropharyngeal swabs were taken at 2-, 4-, 6-, 8-, and 10-days post exposure. Infectious virus was
128 detected in swabs obtained from all exposed animals, except for the two surviving animals in the 10^2 dose
129 VN1203 group. At 2-, 4-, and 6-days post exposure, virus shedding was higher in the 10^2 dose Bov342
130 animals compared to the 10^2 dose VN1203 animals. Significant differences in shedding between virus

131 isolates for both the 10^3 and 10^4 dose groups were only observed on 4 days post exposure (**Figure 1e**). At
132 3 days post exposure, and when endpoint criteria were reached for at least one animal per virus (5 days
133 post exposure for Bov342, and 6 days post exposure for VN1203), tissues were collected from 8 animals
134 per group. Of four animals per group in the 10^4 and 10^2 dose groups only, relative lung weight was
135 measured. Higher relative lung weight is indicative of fluid presence in the lung. At 3 days post exposure
136 and at endpoint, a significant difference in relative lung weight was observed between the animals
137 exposed to 10^2 or 10^4 $TCID_{50}$ Bov342, whereas this was only observed at endpoint in animals inoculated
138 with VN1203. No differences were observed between Bov342 and VN1203 when same dose inoculations
139 were compared (**Supplementary Figure 1b**). Infectious virus titers were measured in brain, nasal
140 turbinate, and lung tissues at 3 days post exposure and at endpoint. In line with the clinical signs that were
141 observed, high viral titers were detected in brain tissue of animals that were inoculated with Bov342 (22
142 out of 24 animals tested positive). Viral titers were significantly lower in animals inoculated with 10^4 dose
143 VN1203 on day 3 and at endpoint, and for 10^2 and 10^3 dose VN1203 at endpoint (10 out of 24 animals
144 tested positive). In contrast, infectious virus was detected in lung tissue of the majority of HPAI H5N1
145 exposed animals regardless of isolate (46 out of 48 animals). Significant differences in virus titer in lung
146 tissue between virus isolates were noted in 10^3 and 10^4 dose groups at endpoint, but not at 3 days post
147 inoculation. Infection of nasal turbinates mirrored that of brain tissue; 21 out of 24 tissues of animals
148 inoculated with Bov342 were positive, whereas 11 out of 24 tissues of animals inoculated with VN1203
149 tested positive, and titers were higher in animals exposed to Bov342 (**Figure 1f**).
150
151 *C57BL/6J mice inoculated with HPAI H5N1 exhibited differential cytokine and chemokine responses*
152 *corresponding with virus isolate, time of necropsy, and inoculum dose.*
153 We then investigated cytokine and chemokine expression in brain, nasal turbinate, and lung tissues
154 obtained from the 10^2 and 10^4 dose groups. In the brain (**Figure 2a and Supplementary Figure 2a**),
155 infection with Bov342 induced the expression of type-I (*Ifna4*, *Ifnb*), -II (*Ifng*), and -III (*Ifnl2*) interferons
156 (IFN), interferon stimulated genes (ISGs) (*Isg15*, *Ifit1*, *Mx1*, *Oas1*), and pro-inflammatory cytokines

157 (*Il1b*, *Il6*, and *Tnfa*) at endpoint. The magnitude of induction was increased at endpoint compared to day 3
158 for *Ifna4*, *Ifng*, *Il6*, *Tnfa*, and ISGs, and expression was dose-dependent for *Ifna4*, *Infg*, and *Tnfa*. With the
159 exception of *Ifna4*, the evaluated genes were not induced in the brain of mice infected with VN1203.
160 Further, at endpoint, expression of *Ifna4*, *Ifng*, *Il1b*, *Il6*, *Tnfa*, and ISGs were significantly higher in mice
161 infected with Bov342 than VN1203.
162 The gene expression changes in nasal turbinates mirrored those observed in the brain. Infection with 10^4
163 dose Bov342 induced type-I, -II, and -III IFN, ISGs, and pro-inflammatory cytokines at the endpoint, but
164 infection with either 10^2 or 10^4 dose of VN1203 did not induce differential expression of any genes
165 assessed (**Figure 2b and Supplementary figure 2b**). Due to insufficient nasal turbinate sample for one
166 of the 10^2 dose Bov342-exposed mice and variability within its endpoint group, we were unable to
167 statistically determine dose-dependent differences.
168 Within the lungs of mice challenged with 10^4 $TCID_{50}$ VN1203, type-I, -II, and -III IFN, ISGs, and pro-
169 inflammatory cytokines genes were induced at day 3 and stayed elevated or decreased in expression at
170 endpoint (**Figure 2c and Supplementary Figure 2c**). Exposure to 10^2 dose VN1203 did not induce
171 expression of any genes uniformly at either timepoint, and induction of *Ifng, Isg15*, and *Tnfa* were
172 significantly lower than mice challenged with 10^4 $TCID_{50}$ VN1203. Virus-dependent differences in gene
173 expression were less apparent in the lung than in the other tissues. Although none of the differences were
174 statistically significant, *Ifng* expression in mice infected with Bov342 tended to be lower than those with
175 VN1203.
176 Protein levels of cytokines and chemokines were then assessed in brain, nasal turbinate, and lung tissue
177 across all dose groups (**Figure 2 and Supplementary Figure 2**). In both brain and nasal turbinate tissues
178 from animals exposed to Bov342, but not VN1203, we detected a dose-dependent expression of CXCL1,
179 IL-1β, IL-6, and TNF-α at endpoint.
180 In lung tissue of Bov342-exposed animals, a dose-dependent elevation of CXCL1 and TNF-α was
181 observed, particularly in tissues collected at endpoint. In contrast, elevated levels of IFN-γ, IL-2, IL-5, IL-
182 10, and TNF-α were detected in lung tissue obtained from animals exposed to VN1203 at endpoint.

183 We then performed Principal Component Analysis (PCA) of viral titer, protein abundance, and mRNA
184 levels in the brain, lung, and nasal turbinates of mice, separated by day of harvest (**Figure 3**). Analysis at
185 3 days post inoculation resulted in two distinct clusters: the smaller cluster contained only lung samples,
186 all but one of which were high dose groups. The remaining low-dose lung samples, all brain, and all nasal
187 samples were contained in the larger cluster.
188 In the PCA of samples collected at endpoint, the optimal number of clusters was determined to be three,
189 with clusters similar in size. One cluster was primarily composed of VN1203-exposed samples, while a
190 second cluster mainly contained Bov342-exposed samples, both predominantly from brain and nasal
191 turbinate samples. The third cluster contained only lung samples, where all but one of the VN1203-
192 exposed mice clustered together with most of the high-dose Bov342-exposed mice. Most of the low-dose
193 Bov342-exposed lung tissues clustered with the Bov342-exposed brain and nasal samples.
194
195 *Histopathologic lung lesions are similar in C57BL/6J mice exposed to both H5N1 isolates and influenza*
196 *A NP immunoreactivity distribution is virus-dependent.*
197 Histologically, pathology was primarily observed in the lungs in both Bov342 and VN1203-exposed
198 animals (**Figure 4a**). At 3 days post exposure, animals exposed to the 10^4 dose of both isolates had
199 developed pulmonary lesions, with lesions being more severe in the Bov342-exposed animals (**Figure**
200 **4a**). At endpoint, for the 10^4 dose for both isolates, histologic lesions were similar to those observed at
201 the 3 days post exposure timepoint **(Figure 4a**). Animals exposed to 10^2 $TCID_{50}$ of Bov342 did not have
202 any pulmonary lesions at 3 days post exposure or endpoint (**Figure 4a**). VN1203-exposed animals in the
203 10^2 dose group did not have pulmonary lesions at 3 days post exposure, however, at endpoint two of the
204 four animals had developed moderate pulmonary lesions (**Figure 4a**). The most common finding in all
205 groups was an acute, moderate to severe, multifocal, necrotizing bronchiolitis, characterized by erosion
206 and ulceration of the bronchiolar epithelium and abundant degenerate cellular debris and fibrin within the
207 bronchiolar lumen, occasionally forming occlusive plugs (**Supplementary Figure 3a**). Multifocal,
208 moderate, bronchointerstitial pneumonia was also observed, characterized by lymphoplasmacytic

209 infiltrates within the peribronchiolar space and expanding the surrounding alveolar septa
210 (**Supplementary Figure 3a**). On immunohistochemistry for influenza A virus NP in the lungs, in both
211 Bov342 and VN1203 animals in the 10^4 dose groups, animals were given a moderate semiquantitative
212 score at 3 days post exposure and a higher score at endpoint (**Figure 4b**). In the 10^2 dose Bov342 animals,
213 two of the four animals had mild to moderate immunoreactivity at 3 days post exposure, and at endpoint
214 one of four animals had marked IHC positivity. In the 10^2 dose VN1203 group, only one animal from
215 both 3 days post exposure and endpoint displayed moderate IHC positivity (**Figure 4b**). Intranuclear and
216 intracytoplasmic immunoreactivity in all groups was primarily within bronchiolar epithelium, and
217 necrotic debris within airway lumen (**Figure 4c**). Immunoreactivity was observed in the nasal respiratory
218 epithelium primarily in the 10^4 dose Bov342 animals at both 3 days post exposure and at endpoint
219 (**Figure 4d**). Immunoreactivity also extended into alveoli, with both type I and type II pneumocytes being
220 infected (**Figure 4c**). Immunoreactivity in pneumocytes was typically not associated with observed
221 pathology (**Figure 4c**).
222 Histologic lesions were not observed for animals exposed to either isolate in nasal turbinates or the brain
223 with the exception of one animal in the 10^2 dose Bov342 group at 3 days post exposure, where very mild
224 acute lesions were observed in the olfactory neuroepithelium and olfactory bulb **(Supplementary Figure**
225 **3b**). The olfactory neuroepithelium in the 10^4 dose Bov342 animals was moderately positive on IHC
226 (**Figure 4d, 4f**). In the brain, immunoreactivity was marked in the 10^4 dose Bov342 animals at endpoint,
227 with all regions of the brain being affected despite the complete lack of pathologic lesions (**Figure 4e, 4f**).
228 Immunoreactivity in the nasal turbinates and brain of the 10^2 dose Bov342 group and all VN1203 groups
229 was rare (**Figure 4d, 4e**). Interestingly, immunoreactivity was observed in other tissues in the head, which
230 were occasionally captured in the sagittal sections. In multiple 10^4 dose Bov342 animals, influenza A
231 virus NP antigen was sporadically observed in the choroid plexus and ependymal cells lining the ventricle
232 (**Supplementary Figure 4a**), cranial nerve nuclei along the ventral aspect of the calvarium
233 (**Supplementary Figure 4b**), multiple cell layers of the retina (**Supplementary Figure 4c**), skeletal
234 myocytes (**Supplementary Figure 4d**), mucosal epithelium overlying the hard palate (**Supplementary**

235 **Figure 4e**), and within brown adipocytes (**Supplementary Figure 4f**). In a single 10^4 dose Bov342
236 animal, immunoreactivity was observed in the dental pulp and overlying odontoblasts of a tooth root
237 (**Supplementary Figure 4g**). In one 10^2 dose VN1203 animal, epithelial cells lining the inner ear were
238 immunoreactive (**Supplementary Figure 4h**). Importantly, the immunoreactivity in all these sites was
239 both intranuclear and intracytoplasmic, indicating virus replication in these tissues.

240 **Discussion**

241 In the current manuscript, we show that exposure to HPAI H5N1-containing aerosols results in productive
242 virus replication in C57BL/6J mice, regardless of whether animals were exposed to HPAI H5N1 strain
243 VN1203 or bovine isolate Bov342. We utilized three different exposure doses, ranging from
244 approximately 10^2 to 10^4 per animal. Importantly, all animals in which evidence of H5N1 virus replication
245 was detected reached endpoint criteria; only two animals in the low-dose VN1203 group did not reach
246 endpoint criteria and did not seroconvert, suggesting they were likely not infected upon exposure. This is
247 supported by the histologic findings, wherein only two of the four 10^2 dose VN1203 animals developed
248 significant pulmonary lesions. This study is not powered to define a 50% infectious dose (ID50), but
249 based on these results, it is likely that the ID50 of VN1203 via aerosol exposure in C57BL/6J mice is
250 around 10^2 $TCID_{50}$. Additionally, it appears that productive infection is 100% lethal in this model.
251 One out of two survivors did not show any evidence of seropositivity. This animal was co-housed with the
252 second survivor (which was seropositive for NA, but not HA) and a third H5N1 VN1203-exposed mouse
253 for the entirety of the experiment. Although this third animal reached endpoint criteria at 10 days post
254 exposure and infectious virus was detected in three out of five oropharyngeal swabs, no evidence of
255 H5N1 transmission to the seronegative mouse was detected. This observation aligns with a recent study,
256 in which no transmission of a bovine isolate of H5N1 was observed between adult mice, whereas
257 transmission from infected mother to pups was detected (18).
258 The most striking finding in this study was the differing tissue tropism between animals exposed to
259 VN1203 and Bov342. Only Bov342-exposed animals exhibited productive virus replication in brain and
260 nasal turbinate tissue, accompanied by signs of CNS infection and distinct cytokine and chemokine
261 profiles. A recent study involving the inoculation of 6-week-old C57BL/6J mice with VN1203 and
262 Bov342 via intranasal and oral routes also reported a CNS tropism for Bov342, but not for VN1203 (21).
263 This contrasts with other studies where VN1203 was found to infect brain and nasal turbinate tissue (17-
264 19). In two of these studies, BALB/cJ mice were inoculated via the intranasal route, whereas in our study
265 C57BL/6J mice were exposed via aerosols, and therefore, the observed tropism may be mouse strain

266 dependent or inoculation route dependent. It is well known that different inoculation routes will alter
267 where the virus starts initial replication (22-24). Interestingly, in a SARS-CoV-2 mouse model in which
268 the human receptor is overexpressed in all tissues, exposure via aerosols results in respiratory disease but
269 no neurological invasion, like we observe with VN1203. In contrast, inoculation via the intranasal route
270 results in both respiratory and neurological disease (25). Contrastingly, in an inoculation route
271 comparison study in which BALB/c mice were inoculated with either HPAI H5N1, LPAI H7N9, or 2009
272 H1N1 via aerosol exposure or direct intranasal inoculation, no differences in lethality were observed
273 based on inoculation route (26). Notably, bovine H5N1 was not neurotropic in BALB/c mice and no
274 neurological signs of disease were described, in contrast to bovine H5N1 in C57BL/6J mice (18, 21),
275 arguing that the observed difference may be mouse strain dependent rather than inoculation route
276 dependent.
277 A previous study showed that H5N1's tropism for the nasal turbinate in BALB/c mice is influenced by the
278 amino acid at position 627 in PB2: a lysine (K) at this position promotes replication in the nasal turbinates
279 and lungs, while a glutamic acid (E) restricts it (19). Likewise, a secondary study showed the selection of
280 627K within HPAI H5N1 in the respiratory tract of a mouse model, and an increase in virus replication in
281 the upper and lower respiratory tract associated with this mutation (17). In our study, VN1203, which
282 contains the amino acid PB2 627K, displays restricted virus replication in the nasal turbinates compared
283 to Bov342, but replicates effectively in lung tissue. Other animal models also do not show a clear
284 difference in virus replication based on the PB2 E627K mutation. In ferrets, no differences in shedding
285 from the upper respiratory tract was noted between reverse genetics viruses only differing by the PB2 627
286 amino acid, and PB2 627E was stable in a ferret serial passage study (27). In guinea pigs, no major
287 differences were found in transmission of VN1203 with PB2 627K or 627E. Additionally, introduction of
288 the PB2 627E mutation in a H3N2 isolate only resulted in moderate differences in virus replication in the
289 upper and lower respiratory tract compared to H3N2 containing PB2 627K (20). Thus, tissue tropism may
290 vary depending on the animal model used.

291 HPAI H5Nx infection differs from other influenza A viruses as it has a significantly higher likelihood of
292 leading to CNS infection within mammalian hosts (Reviewed in (28)). For example, experimental
293 infection of cats via intratracheal inoculation or feeding on H5N1-infected chicks resulted in infection of
294 multiple regions of the brain (29). In contrast, CNS involvement has not yet been reported for dairy cows,
295 either via natural or experimental infection. It has been hypothesized that H5N1 transmission within and
296 between cattle herds is associated with milking practices. HPAI H5N1 replication was limited to the
297 mammary glands when lactating cows were inoculated via the mammary gland (30). Thus, CNS
298 involvement may be associated with efficient replication in the respiratory tract. In our study, CNS
299 involvement of VN1203-inoculated animals was limited, and so was replication the upper respiratory
300 tract.
301 Unsurprisingly, we detected significant differences in cytokine and chemokine profiles in brain and nasal
302 turbinate tissues when comparing Bov342 and VN1203 at endpoint: induction of cytokines and
303 chemokines was mostly limited to tissues obtained from animals exposed to Bov342 in which extensive
304 virus replication was found. However, despite similar virus replication in lung tissue, significantly
305 different cytokine and chemokine profiles were found between Bov342 and VN1203-exposed animals at
306 protein level. Bov342 infection resulted in upregulation of CXCL1, whereas VN1203 resulted in IFN-γ,
307 IL-2, IL-5, and IL-10. At the RNA level, gene expression was relatively similar between isolates. PCA
308 showed clustering of the majority of lung samples, independent of virus isolate exposure, and histologic
309 examination of the lungs did not reveal any striking differences between Bov342 and VN1203, both
310 isolates caused a similar necrotizing bronchiolitis to bronchointerstitial pneumonia. It should be noted that
311 differences may be time-related, Bov342-exposed animals reached endpoint at 5 days post exposure, and
312 VN1203-exposed animals reached endpoint criteria at 6 days post exposure. More detailed analyses
313 would be needed to confirm these findings and identify mechanisms of induction.
314 The key histologic differences between VN1203 and Bov342 exposure was observed in the olfactory
315 neuroepithelium and CNS. By examining sagittal sections of the whole head in these H5N1-exposed
316 animals, we were able to visualize the distribution of viral antigen in the nasal turbinates and brain in

317 relation to one another. In the Bov342 animals, there was extensive virus antigen observed in the olfactory
318 neuroepithelium, olfactory bulb, and scattered throughout other regions of the brain. Given the consistent
319 and abundant immunoreactivity in the olfactory tissues, extension of the virus from the olfactory
320 neuroepithelium through the nerves to the olfactory bulb seems most likely. This is supported by
321 occasional NP antigen being observed in olfactory nerves. However, the presence of NP antigen in
322 random foci throughout the CNS, distant from the olfactory bulb, and other tissues in the head suggest
323 hematogenous dissemination might also plays a role. While histopathologic lesions were not observed in
324 these areas of abundant immunoreactivity, the alterations in cytokine profiles in these animals compared
325 to the VN1203 group indicates a cellular response. As these animals were euthanized prior to the onset of
326 severe neurologic disease, it may be that histologic lesions would develop later. A publication describing
327 the examination of cats who had died on dairy farms, and later tested positive for H5N1, had a severe
328 meningoencephalitis and chorioretinitis (11). Interestingly, viral antigen was found not only in the CNS
329 Bov342-exposed animals, but also within the retina.
330 The potential consequences of viral antigen in various tissues not typically associated with influenza A
331 virus replication is unknown. To the author's knowledge, influenza A antigen has not been documented in
332 some of these sites, which could either be a function of not assessing these sites on routine sample
333 collection or uniquely wide tropism of Bov342 in this mouse model. While we did not observe any
334 pathology in these unexpected sites of virus antigen, further investigation into potential sequalae is
335 warranted. Of particular interest to the authors is the presences of viral antigen in the choroid plexus,
336 where virus may be shed into the cerebral spinal fluid. Additional animal studies evaluating neurotropism
337 of Bov342 should consider evaluating the CSF and spinal cord for viral load and histology.
338 In conclusion, we show efficient virus replication of H5N1 strains VN1203 and Bov342 in C57BL/6J
339 mice upon aerosol exposure. In this study, Bov342 displays a neurotropic profile, whereas both viruses
340 replicate efficiently in the lower respiratory tract. Surprisingly, differing cytokine profiles can be detected
341 in lung tissue at endpoint, dependent on virus isolate. Importantly, the findings in this study appear to be
342 mouse specific and likely not representative of what will occur in humans, as thus far there is no evidence

343 of CNS infection in contemporary H5N1 patients. Understanding the strain differences in the context of
344 the mouse model is still of great value and these models will be essential for the evaluation of vaccines
345 and antivirals.
346

347 **Methods**

348 *Ethics statement*

349 Mouse studies were performed in an AAALAC International-accredited facility and approved by the
350 Rocky Mountain Laboratories Institutional Care and Use Committee following the guidelines put forth in
351 the Guide for the Care and Use of Laboratory Animals 8th edition, the Animal Welfare Act, United States
352 Department of Agriculture and the United States Public Health Service Policy on the Humane Care and
353 Use of Laboratory Animals.

354 The Institutional Biosafety Committee (IBC) approved work with highly pathogenic H5N1 avian
355 influenza viruses under BSL3 conditions. Virus inactivation of all samples was performed according to
356 IBC-approved standard operating procedures for the removal of specimens from high containment areas.

357

358 *Cells and Viruses*

359 Bovine HPAI H5N1 isolate A/Bovine/Ohio/B24osu-342/2024 (EPI_ISL_678615) was obtained from
360 Richard Webby at St. Jude's Children hospital, Memphis, TN, USA and Andrew Bowman at Ohio State
361 University, Columbus, OH, USA. Human HPAI H5N1 isolate A/Vietnam/1203/2004 was obtained from
362 Dr. Kanta Subbarao at the Peter Doherty Institute, Melbourne, Australia.

363 Virus propagation was performed in Madin-Darby canine kidney (MDCK) cells in MEM supplemented
364 with 1 mM L-glutamine, 50 U/mL penicillin, 50 µg/mL streptomycin, 1x NEAA, 20 mM HEPES, and 4
365 µg/mL TPCK trypsin. MDCK cells were maintained in MEM supplemented with 10% fetal bovine serum,
366 1 mM L-glutamine, 50 U/ml penicillin, and 50 µg/ml streptomycin, 1x NEAA, 20 mM HEPES.
367 Mycoplasma testing is performed at regular intervals. No mycoplasma was detected during the study.

368

369 *Animal studies*

370 Six groups of C57BL/6J mice (Jackson Laboratories, strain #000664, between 6-8 weeks old) were
371 challenged with HPAI H5N1 via aerosols (see details below), resulting in an estimated total dose of 2.4 x
372 10^2, 5.4 x 10^2, or 1.2 x 10^4 $TCID_{50}$/animal for A/Bovine/Ohio/B24osu-342/2024, and 2.5 x 10^2, 7.8 x 10^2,

373 or 3.6 x 10^3 $TCID_{50}$/animal for A/Vietnam/1203/2004. Prior to challenge, a subgroup of mice was
374 implanted with telemetry transponders (UCT-2112, Unified Information Devices (UID)) via subcutaneous
375 implantation and allowed to rest for three days before challenge. Activity (total inches travelled) was
376 recorded using a UID telemetry system and UID Mouse Matrix Plates. Data was recorded continuously
377 with a zone interval of 250 ms, 2 cycles per series, and a 1s series delay. Oropharyngeal swabs were
378 collected every other day in 1 mL of DMEM containing 2% of FBS, 1 mM L-glutamine, 50 U/mL
379 penicillin, and 50 µg/mL streptomycin up until 10 days post exposure. On day 3 and when endpoint
380 criteria were reached for at least one animal per group, four animals from each group were euthanized.
381 The lungs were excised and weighed, and samples were taken from lung, brain, and nasal turbinate tissues
382 for virus titrations and histopathology. Six animals in each group were monitored at least daily for signs
383 of disease.
384
385 *Virus exposure via aerosols*
386 Aerosol droplet nuclei were generated by a three-jet collision nebulizer (Biaera Technologies), ranging
387 from 1 µm to 5 µm in size. A sample of 6 L of air per min was collected during the 10 min exposure on the
388 47 mm gelatin filter (Sartorius). Post-exposure, the filters were dissolved in 10 mL of DMEM containing
389 10% FBS and infectious virus was titrated, and the aerosol concentration was calculated. The estimated
390 inhaled inoculum was calculated using the respiratory minute volume rates of the animals determined
391 using methods used previously (31). The inhaled dose was calculated using the simplified formula
392 $D = R \times Caero \times Texp$ (32), where D is the inhaled dose, R is the respiratory minute volume ($l\,min^{-1}$),
393 Caero is the aerosol concentration (tissue culture infectious dose, TCID50) and Texp is the duration of the
394 exposure (min). Three different groups were exposed to BoV342 and VN1203 HPAI H5N1 variants. The
395 average doses per BoV342 group are as follows: 2.4 x 10^2, 5.4 x 10^2, and 1.2 x 10^4 $TCID_{50}$. The average
396 doses per VN1203 group are as follows: 2.5 x 10^2, 7.8 x 10^2, and 3.6 x 10^3 $TCID_{50}$.
397
398 *Virus titration*

399 Tissue sections were weighed and homogenized in 1 mL of MEM. Virus titrations were performed by
400 end-point titration of 10-fold dilutions of virus swab media or tissue homogenates on MDCK cells in 96-
401 well plates. When titrating tissue homogenate, the top 2 rows of cells were washed two times with PBS
402 prior to the addition of a final 100 µl of MEM supplemented with 1 mM L-glutamine, 50 U/mL penicillin,
403 50 µg/mL streptomycin, 1x NEAA, 20 mM HEPES, and 4 µg/mL TPCK trypsin. Cells were incubated at
404 37 °C and 5% CO2. After three days, presence or absence of infectious virus was measured using a HA
405 assay. Turkey red blood cells (IGTKWBNAC50ML, Innovative Research) were ordered weekly. Red
406 blood cells (RBCs) were washed at least three times with PBS and diluted to 0.33% in PBS directly
407 before use. 75 µl of 0.33% RBCs were added to 25 µl of virus and left at 4°C for 1 hour. Hereafter, wells
408 were marked as either agglutinated or negative. Titers were calculated using the Spearman-Karber
409 method.
410
411 *RNA extraction*
412 Tissue samples were bead homogenized and extracted using the RNeasy kit (Qiagen) according to the
413 manufacturer's instructions and following high containment laboratory protocols.
414
415 *Quantitative reverse-transcription polymerase chain reaction*
416 Following extraction, 17 µL of RNA from nasal turbinates, lung, and brain samples were treated with
417 TURBO DNase (Invitrogen) according to the manufacturer's instructions. After DNase treatment, the
418 RNA was diluted 1:5 in molecular grade water (Invitrogen). DNase-treated RNA (5 µL) was used for each
419 host gene assessed (**Supplementary Table 1**). Fold change was calculated for host genes by dividing the
420 sample relative gene expression by the average relative gene expression of the healthy controls (ΔΔCt)
421 and then $\log_2$ transformed.
422
423 *Measurement of cytokines and chemokines protein levels in tissues*

424 Tissue samples were bead homogenized in 1 mL of MEM and spun for 10 min at 8000 x rcf. 150 μL of
425 supernatant was inactivated with γ-irradiation (8 MRad) according to standard operating procedures.
426 Tissue supernatants were assayed using the MSD Technology V-PLEX Proinflammatory Panel 1 Mouse
427 kit (K-15048D, includes CXCL1, IFN-γ, IL-1β, IL-2, IL-4, IL-5, IL-6, IL-10, IL-12p70, and TNFα)
428 according to the manufacturer's instructions. Analysis was performed using Discovery Workbench
429 LSR_4_0_13 Software.
430
431 *Histology and immunohistochemistry*
432 All tissues harvested at the time of necropsy were fixed in 10% neutral-buffered formalin for ≥7 days.
433 Hematoxylin and eosin (H&E) staining, and immunohistochemistry (IHC) were performed on formalin-
434 fixed paraffin-embedded (FFPE) tissue sections. Immunoreactivity was detected using Millipore Sigma
435 Anti-Influenza A nucleoprotein antibody (Cat.#ABF1820-25UL) at a 1:12,000 dilution. Roche Tissue
436 Diagnostics DISCOVERY Omnimap anti-rabbit HRP (#760-4311) was used as a secondary antibody. For
437 negative controls, replicate sections from each control block were stained in parallel following an
438 identical protocol, with the primary antibody replaced by Vector Laboratories rabbit IgG (#I-1000-5) at a
439 1:2500 dilution. The tissues were stained using the DISCOVERY ULTRA automated stainer (Ventana
440 Medical Systems) with a Roche Tissue Diagnostics DISCOVERY purple kit (#760-229).
441 Histologic lesions from the brain, nasal turbinates and lung were categorized and scored by a board-
442 certified veterinary pathologist blinded to group allocations (**Supplementary Table 2**). For each category,
443 histological lesions were scored on the scale of 0 = none, 1 = rare, 2 = mild, 3 = moderate and 4 = severe.
444 Immunohistochemistry scoring was as follows 0 = none/no positive cells; 1 = rare positive cells; 2 = few
445 positive cells; 3 = moderate numbers of positive cells; 4 = abundant positive cells. A representative lesion
446 from each group was selected for figures.
447
448 *Enzyme-linked immunosorbent assay*

449 Nunc MaxiSorp flat bottom 96-well plates (ThermoFisher Scientific) were coated with 50 ng in 50
450 µl/well of influenza A H5N1 A/Vietnam/1203/2004 hemagglutinin (HA) protein (IBT Bioservices, 1501-
451 001), or A/bald eagle/Florida/W22-134-OP/2022 neuraminidase (NA) protein (BEI Resources, NR-
452 59476), blocked with 100 µL of casein in PBS (ThermoFisher Scientific), and incubated with serially
453 diluted mouse sera (1:100-1:512000) in duplicate. Immunoglobulin G (IgG) antibodies were detected by
454 using affinity-purified polyclonal antibody peroxidase-labeled donkey-anti mice IgG (Jackson
455 Immunoresearch, 715-035-151) or affinity-purified polyclonal antibody peroxidase-labeled goat anti-
456 monkey IgG (ThermoFisher Scientific, PA1-84631) at a dilution of 1:5000 in casein followed by 3,3′,5,5′-
457 Tetramethylbenzidine 2-component peroxidase substrate (Seracare, 5120–0047) and stop solution
458 (Seracare, 5150-0021). The optical density at 450 nm (OD450) was then measured. Wells were washed
459 three times with PBS containing 0.1% Tween in between each step.
460
461 *Statistical Analysis*
462 Principal Component Analysis (PCA) was run at day 3 and endpoint, and included viral titer, protein
463 abundances, and mRNA levels in brain, lung, and nasal turbinate samples with all data $\log_{10}$ transformed.
464 Variables with more than 10% missingness (IFNβ and IFN-l2 mRNA levels) or with low variability
465 (IL12p70, IL-4, and IL-2 protein abundance) were dropped from PCA analyses, and the remaining
466 missing observations were imputed using Multiple Imputation by Chained Equations (MICE) (33). The
467 number of clusters for each PCA were determined by the majority vote of 26 commonly used indices for
468 identifying the optimal number of clusters under k-means clustering (34), and k-means clusters were
469 calculated for each PCA. PCA analyses and visualizations were run in R version 4.4.1.
470 All other statistical analysis were performed in Graphpad Prism using a two-way ANOVA followed by a
471 Mann-Whitney test. Gene expression differences between viruses and dose were compared at day 3 and
472 endpoint using a two-way ANOVA with Tukey's post-test, and differences across time points were assess
473 with a two-way ANOVA with Sidak's multiple comparisons test. A Bonferroni correction was applied,
474 and only p-values greater than 0.0044 were considered significant.

Data Availability Statement

All data have been deposited on Figshare: 10.6084/m9.figshare.27679509. All code has been deposited on Github: https://github.com/IDSS-NIAID/2024-H5N1-comparisons-in-mice.

Funding Statement

This work was supported by the Intramural Research Program of the National Institute of Allergy and Infectious Diseases (NIAID), National Institutes of Health (NIH).

Acknowledgements

We thank the animal caretakers of the Rocky Mountain Veterinary Branch, NIAID, NIH for their assistance during the study, Dean Follmann for advice on appropriate statistical analysis, Andrea Marzi and Kyle O'Donnell for providing controls and reagents for the ELISA assay, and Anita Mora for assistance with figures.

490 **REFERENCES**

491 1. E. J. Elsmo *et al.*, Highly Pathogenic Avian Influenza A(H5N1) Virus Clade 2.3.4.4b Infections in
492 Wild Terrestrial Mammals, United States, 2022. *Emerg Infect Dis* **29**, 2451-2460 (2023).
493 2. M. Agüero *et al.*, Highly pathogenic avian influenza A(H5N1) virus infection in farmed minks,
494 Spain, October 2022. *Eurosurveillance* **28**, 2300001 (2023).
495 3. P. I. Plaza, V. Gamarra-Toledo, J. Rodriguez Eugui, N. Rosciano, S. A. Lambertucci, Pacific and
496 Atlantic sea lion mortality caused by highly pathogenic Avian Influenza A(H5N1) in South
497 America. *Travel Med Infect Dis* **59**, 102712 (2024).
498 4. E. C. Claas *et al.*, Human influenza A H5N1 virus related to a highly pathogenic avian influenza
499 virus. *Lancet* **351**, 472-477 (1998).
500 5. K. S. Li *et al.*, Genesis of a highly pathogenic and potentially pandemic H5N1 influenza virus in
501 eastern Asia. *Nature* **430**, 209-213 (2004).
502 6. R. Harfoot, R. J. Webby, H5 influenza, a global update. *J Microbiol* **55**, 196-203 (2017).
503 7. T. H. Tran *et al.*, Avian influenza A (H5N1) in 10 patients in Vietnam. *N Engl J Med* **350**, 1179-
504 1188 (2004).
505 8. T. Chotpitayasunondh *et al.*, Human disease from influenza A (H5N1), Thailand, 2004. *Emerg*
506 *Infect Dis* **11**, 201-209 (2005).
507 9. A. Kandeil *et al.*, Rapid evolution of A(H5N1) influenza viruses after intercontinental spread to
508 North America. *Nat Commun* **14**, 3082 (2023).
509 10. W. Puryear *et al.*, Highly Pathogenic Avian Influenza A(H5N1) Virus Outbreak in New England
510 Seals, United States. *Emerg Infect Dis* **29**, 786-791 (2023).
511 11. E. R. Burrough *et al.*, Highly Pathogenic Avian Influenza A(H5N1) Clade 2.3.4.4b Virus
512 Infection in Domestic Dairy Cattle and Cats, United States, 2024. *Emerg Infect Dis* **30**, 1335-
513 1343 (2024).
514 12. USDA (2024) https://www.aphis.usda.gov/livestock-poultry-disease/avian/avian-influenza/hpai-
515 detections/hpai-confirmed-cases-livestock.
516 13. CDC (2024) https://www.cdc.gov/bird-flu/situation-summary/index.html.
517 14. A. M. Mellis *et al.*, Serologic Evidence of Recent Infection with Highly Pathogenic Avian
518 Influenza A(H5) Virus Among Dairy Workers — Michigan and Colorado, June–August 2024.
519 *MMWR Morb Mortal Wkly Rep* **73**, 1004-1009 (2024).
520 15. CDC (2024) https://www.cdc.gov/media/releases/2024/s0906-birdflu-case-missouri.html.
521 16. T. R. Maines *et al.*, Avian influenza (H5N1) viruses isolated from humans in Asia in 2004 exhibit
522 increased virulence in mammals. *J Virol* **79**, 11788-11800 (2005).
523 17. J. Y. Min *et al.*, Mammalian adaptation in the PB2 gene of avian H5N1 influenza virus. *J Virol* **87**,
524 10884-10888 (2013).
525 18. A. J. Eisfeld *et al.*, Pathogenicity and transmissibility of bovine H5N1 influenza virus. *Nature*
526 **633**, 426-432 (2024).
527 19. M. Hatta *et al.*, Growth of H5N1 influenza A viruses in the upper respiratory tracts of mice. *PLoS*
528 *Pathog* **3**, 1374-1379 (2007).
529 20. J. Steel, A. C. Lowen, S. Mubareka, P. Palese, Transmission of influenza virus in a mammalian
530 host is increased by PB2 amino acids 627K or 627E/701N. *PLoS Pathog* **5**, e1000252 (2009).
531 21. T. Tipih *et al.*, Recent Bovine HPAI H5N1 Isolate Is Highly Virulent For Mice, Rapidly Causing
532 Acute Pulmonary And Neurologic Disease. *BioRXiv* https://doi.org/10.1101/2024.08.19.608652
533 (2024).
534 22. E. de Wit *et al.*, Foodborne transmission of nipah virus in Syrian hamsters. *PLoS Pathog* **10**,
535 e1004001 (2014).
536 23. T. J. Gregory, H. Irshad, R. Chand, P. J. Kuehl, Deposition of Aerosolized Lucinactant in
537 Nonhuman Primates. *J Aerosol Med Pulm Drug Deliv* **33**, 21-33 (2020).
538 24. M. P. Citron *et al.*, A novel method for strict intranasal delivery of non-replicating RSV vaccines
539 in cotton rats and non-human primates. *Vaccine* **36**, 2876-2885 (2018).

25. V. Fumagalli *et al.*, Administration of aerosolized SARS-CoV-2 to K18-hACE2 mice uncouples respiratory infection from fatal neuroinvasion. *Sci Immunol* **7**, eabl9929 (2022).
26. J. A. Belser, K. M. Gustin, J. M. Katz, T. R. Maines, T. M. Tumpey, Comparison of traditional intranasal and aerosol inhalation inoculation of mice with influenza A viruses. *Virology* **481**, 107-112 (2015).
27. S. Herfst *et al.*, Airborne transmission of influenza A/H5N1 virus between ferrets. *Science* **336**, 1534-1541 (2012).
28. L. Bauer, F. F. W. Benavides, E. J. B. Veldhuis Kroeze, E. de Wit, D. van Riel, The neuropathogenesis of highly pathogenic avian influenza H5Nx viruses in mammalian species including humans. *Trends Neurosci* **46**, 953-970 (2023).
29. G. F. Rimmelzwaan *et al.*, Influenza A virus (H5N1) infection in cats causes systemic disease with potential novel routes of virus spread within and between hosts. *Am J Pathol* **168**, 176-183; quiz 364 (2006).
30. N. J. Halwe *et al.*, H5N1 clade 2.3.4.4b dynamics in experimentally infected calves and cows. *Nature* 10.1038/s41586-024-08063-y (2024).
31. D. J. Alexander *et al.*, Association of Inhalation Toxicologists (AIT) working party recommendation for standard delivered dose calculation and expression in non-clinical aerosol inhalation toxicology studies with pharmaceuticals. *Inhal Toxicol* **20**, 1179-1189 (2008).
32. J. M. Hartings, C. J. Roy, The automated bioaerosol exposure system: preclinical platform development and a respiratory dosimetry application with nonhuman primates. *J Pharmacol Toxicol Methods* **49**, 39-55 (2004).
33. S. van Buuren, K. Groothuis-Oudshoorn, mice: Multivariate Imputation by Chained Equations in R. *Journal of Statistical Software* **45**, 1 - 67 (2011).
34. M. Charrad, N. Ghazzali, V. Boiteau, A. Niknafs, NbClust: An R Package for Determining the Relevant Number of Clusters in a Data Set. *Journal of Statistical Software* **61**, 1 - 36 (2014).

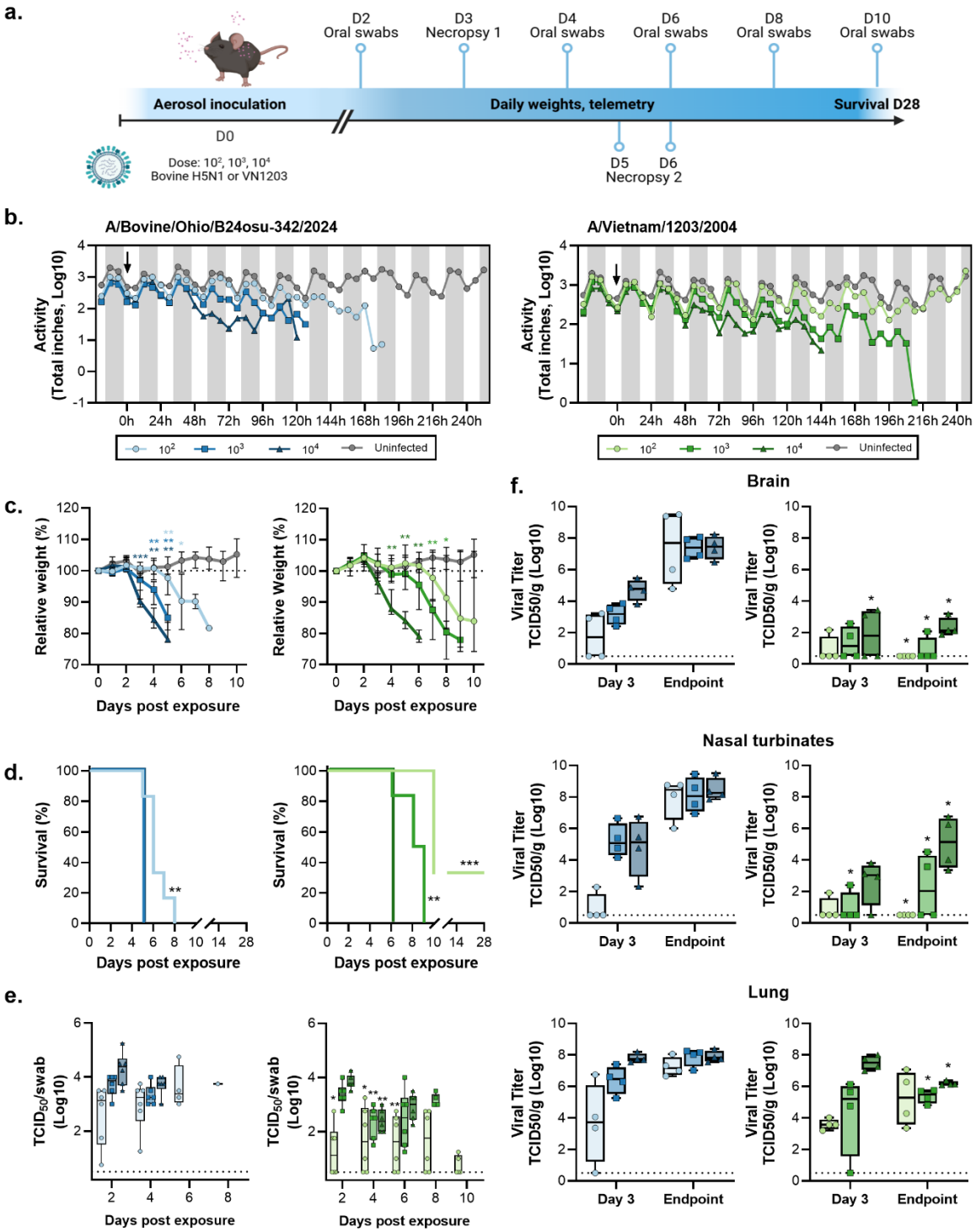

Figure 1. Aerosol inoculation of C57BL/6J mice with H5N1 results in dose-dependent mortality and virus replication. a. Experimental schedule. Mice (N=14) were inoculated with A/Bovine/Ohio/B24osu-342/2024 or A/Vietnam/1203/2004 at 10^2, 10^3, or 10^4 $TCID_{50}$, via aerosols. Oral swabs were taken every two days (N=6), and necropsies were scheduled on D3 and D6 post exposure (N=4). One group per dose

of virus was observed for survival up to D28 post exposure (N=6). Image created using Biorender. b. All animals in the survival groups received a transponder, and activity was monitored up to D10 post inoculation. Activity in inches traveled was totaled per 6 hours, shown is median (N=6). Arrow indicates time of virus exposure via aerosols. c. Relative weight compared to D0 post exposure. Shown is median with 95% confidence interval (CI), weights of all groups were compared to weights of control animals on same day post exposure. d. Survival post virus exposure (N=6). Survival comparison was done against high dose group per virus. e. Shedding profile of infectious virus in oral swabs. Individual values shown, bar graph shows minimum to maximum, with middle line displaying median (N=6). For each day, amount of shedding was compared between BoV342 and VN1203 animals that received the same dose of virus. f. Infectious virus titer in brain, nasal turbinate, and lung tissues at D3 and either D5 (BoV342) or D6 (VN1203) post exposure. Individual values shown, bar graph shows minimum to maximum, with middle line displaying median (N=4). For each day, amount of shedding was compared between BoV342 and VN1203 animals that received the same dose of virus. For statistical analysis in c, e, and f, first a one-way ANOVA (f), two-way ANOVA (c), or mixed-effect analysis (e) was performed. If significantly different, groups of interests were compared using a Mann-Whitney test. Survival was compared via Kaplan-Meier analysis. * = p-value <0.05; ** = p-value <0.01; *** = p-value <0.001.

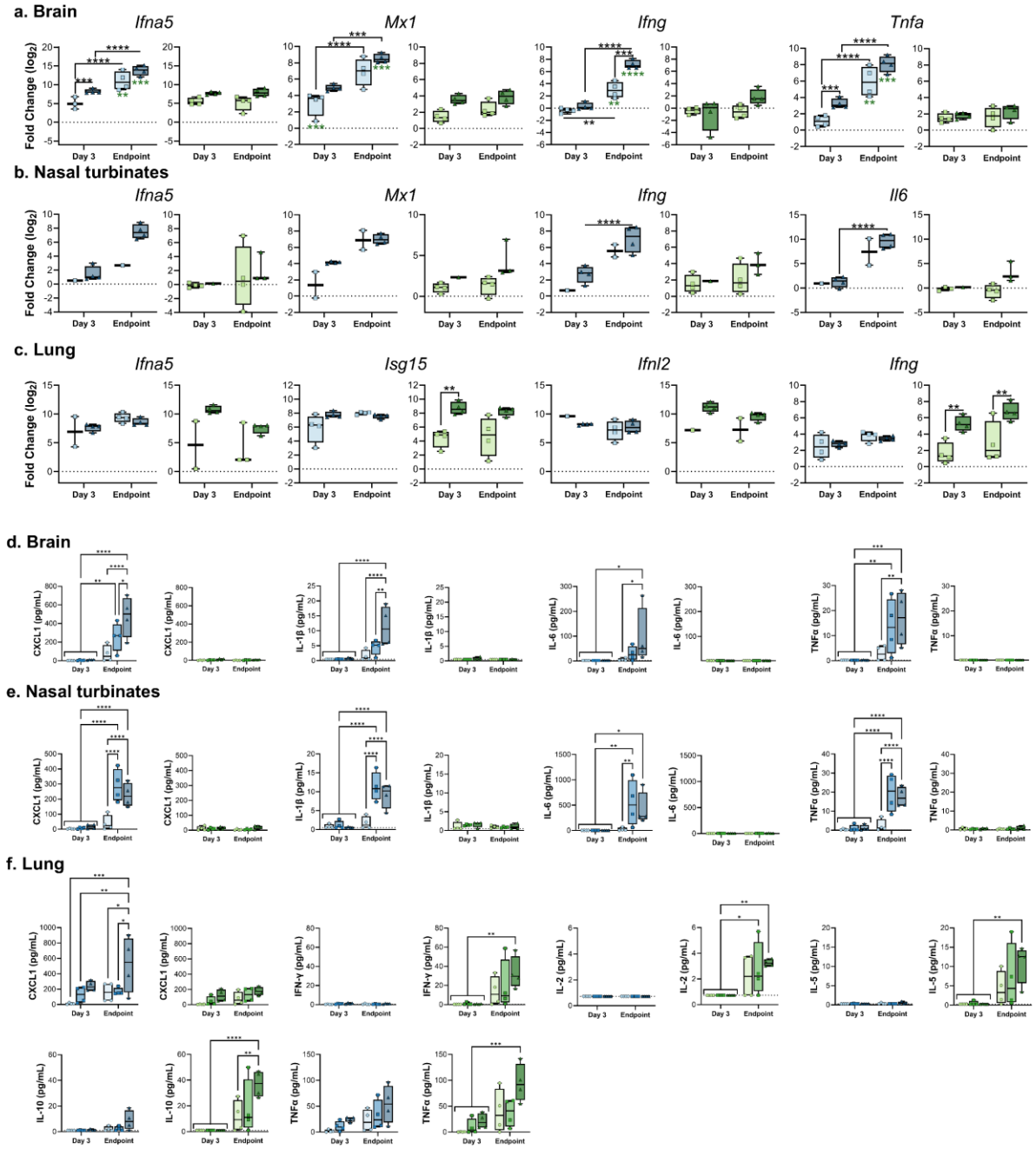

Figure 2. Aerosol inoculation of C57Bl/6J mice with HPAI H5N1 results in virus-, tissue- and dose-dependent induction of cytokines and antiviral effectors. Gene expression in brain (a), nasal turbinate (b), or lung (c) shown as $\log_2$ transformed fold change relative to healthy control mice. Cytokine and chemokine detection in brain (d), nasal turbinate (e), or lung (f) tissue. Individual values shown, bar graph shows minimum to maximum, with middle line displaying median (N=4). Gene expression differences between viruses and dose were compared at day 3 and endpoint using a two-way ANOVA with Tukey's post-test, and differences across time points were assess with a two-way ANOVA with Sidak's multiple comparisons test. A Bonferroni correction was applied, and only p-values greater than 0.0044 were considered significant. **= p-value <0.0044, ***= p-value <0.001, ****=p-value <0.0001.

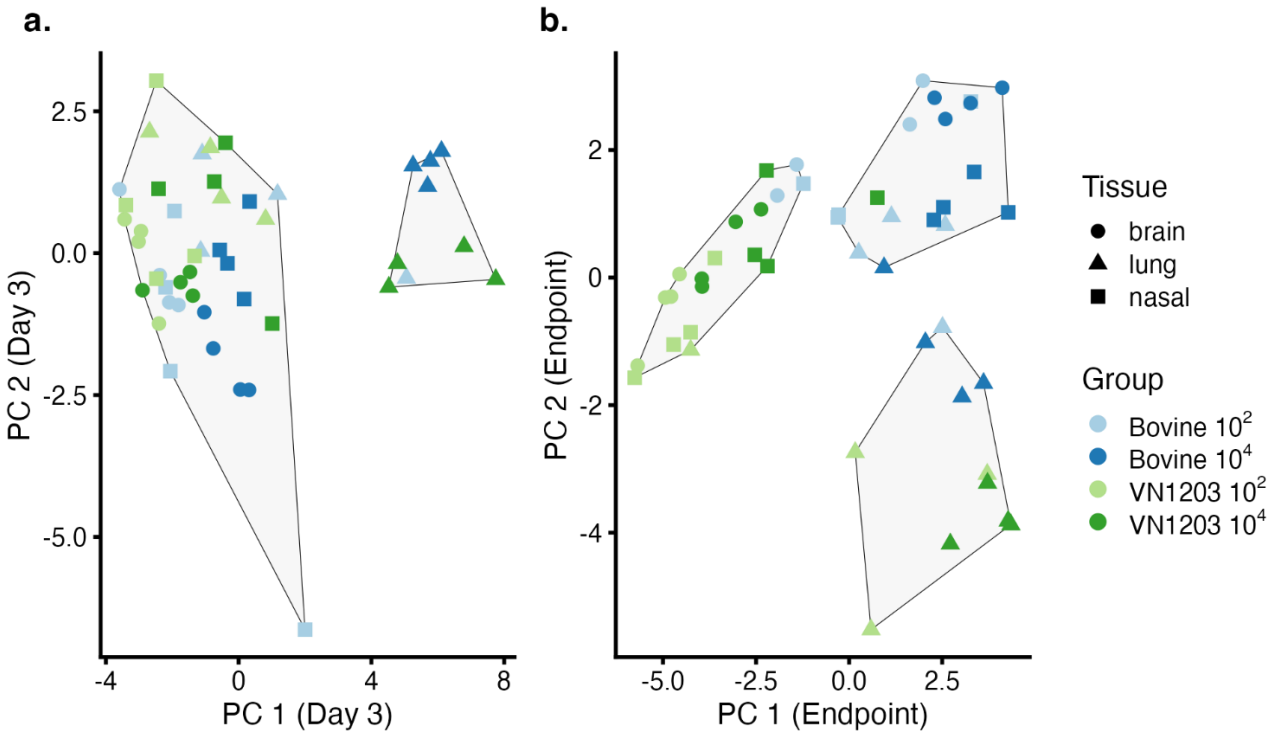

Figure 3. Principal Component Analysis of virus titer, protein abundances, and mRNA levels in mice grouped by tissue, virus, and dose. Principal component analyses are shown for mice at 3 days post inoculation (a) and at endpoint (b) with K-means clusters differentiated by light grey polygons. The optimal number of clusters (two for day 3 and three for endpoint) were identified by the majority vote of 26 indices for determining the number of clusters (1).

1. M. Charrad, N. Ghazzali, V. Boiteau, A. Niknafs, NbClust: An R Package for Determining the Relevant Number of Clusters in a Data Set. *Journal of Statistical Software* **61**, 1 - 36 (2014).

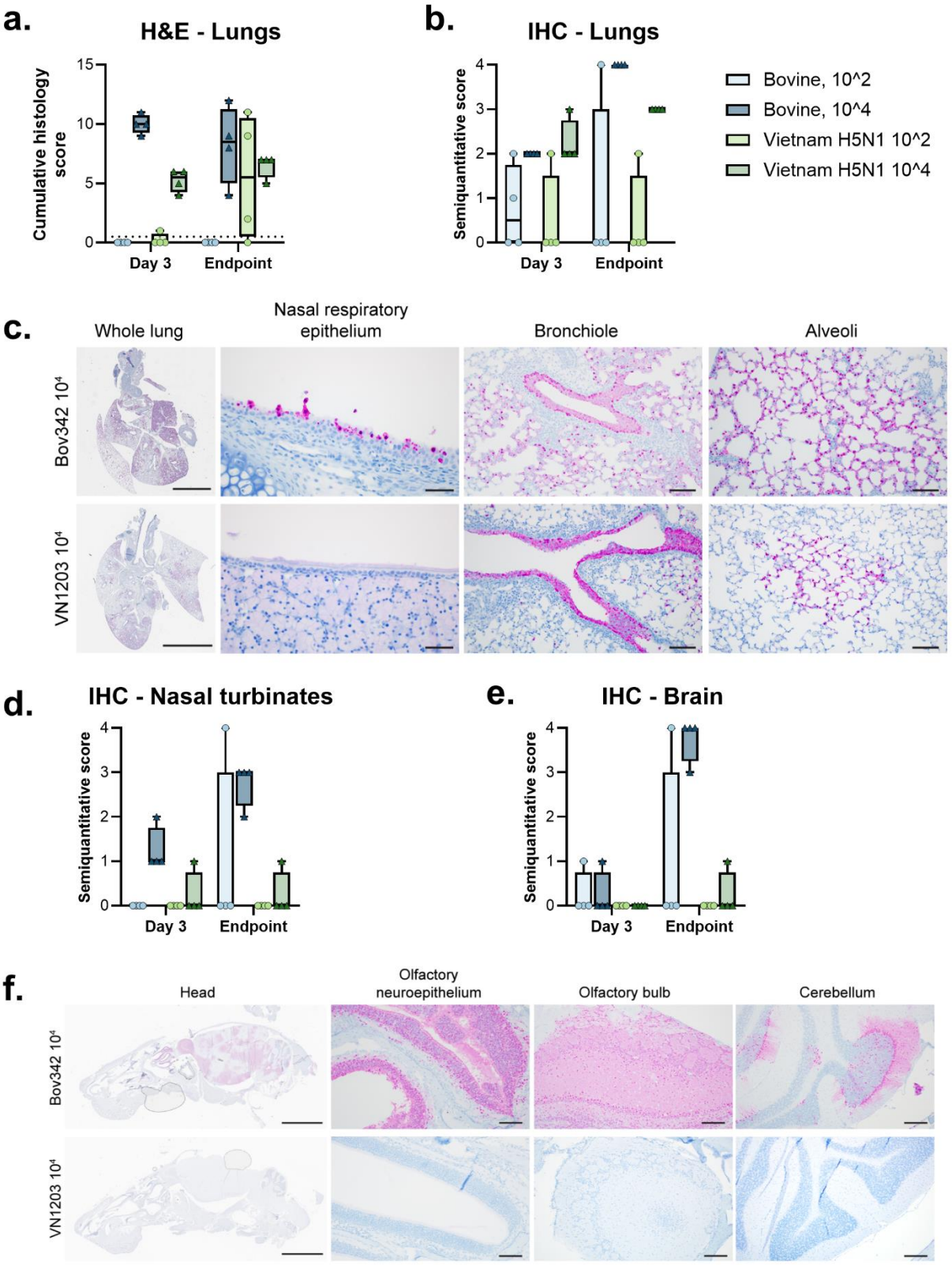
a.
H&E - Lungs
Cumulative histology score
15
10
5
0
Day 3
Endpoint
b.
IHC - Lungs
Semiquantitative score
4
3
2
1
0
Day 3
Endpoint
Bovine, 10^2
Bovine, 10^4
Vietnam H5N1 10^2
Vietnam H5N1 10^4
c.
Whole lung
Nasal respiratory epithelium
Bronchiole
Alveoli
Bov342 10⁴
VN1203 10⁴
d.
IHC - Nasal turbinates
Semiquantitative score
Day 3
Endpoint
e.
IHC - Brain
Semiquantitative score
Day 3
Endpoint
f.
Head
Olfactory neuroepithelium
Olfactory bulb
Cerebellum
Bov342 10⁴
VN1203 10⁴

Figure 4. Aerosol inoculation of C57BL/6J mice with H5N1 results in similar histopathologic lesions in the lungs and virus-dependent IAV NP immunoreactivity in the olfactory epithelium and CNS. . Pulmonary lesions were observed in the Bov342 10^4 group and both VN1203 doses at 3 days post exposure and at endpoint (a). Cumulative histology score calculated by adding semiquantitative values assigned in multiple categories (Table S2) (a). Immunoreactivity for influenza A virus NP (pink) was observed in the lungs in all animals in the 10^4 dose groups for animals at 3 days post exposure and endpoint, however, only observed sporadically in the 10^2 dose groups for both isolates at both timepoints (b). At endpoint, immunoreactivity in the Bov342 10^4 group was observed within the nasal respiratory epithelium and lower airways, including bronchioles and type I and type II pneumocytes. Comparatively, VN1203-exposed animals had similar immunoreactivity in the bronchioles and alveoli and rare positivity in the nasal respiratory epithelium at endpoint (c). Influenza A virus NP positivity was observed in the nasal turbinates of the Bov342 10^4 group at both timepoints, in one Bov342 10^2 animal at endpoint, and in one animal in the VN1203 10^4 group and 3 days post exposure and endpoint (d). At endpoint, immunoreactivity in the brain was observed abundantly in all Bov342 10^4 animals and one animal in the Bov342 10^2 group (e). Immunoreactivity in the Bov342 10^4 animals at endpoint was widely distributed throughout the olfactory neuroepithelium and CNS, including the olfactory bulb and randomly scattered sites throughout the cerebrum, cerebellum, and brainstem (f). VN1203-exposed animals had no significant positivity in the olfactory tissue or CNS (f). For all graphs, individual values shown on boxplots. Whole lung: scale bar=4mm. Nasal respiratory epithelium: scale bar=50µm. Bronchiole: scale bar=100µm. Alveoli: scale bar=100µm Head: scale bar=5mm. Olfactory neuroepithelium: scale bar=100µm. Olfactory bulb: scale bar=200µm. Cerebellum: scale bar=200 µm.

Supplementary Table 1. RT-qPCR primers used to measure host gene expression.

Gene target	Sequence
Ifna5 F	TTTGGATTCCCACAGGAGAAGGT
Ifna5 R	AGGACCTGCTGGGTCAGCTC
Ifna5 P	AGCCTCCTGGATCTGCTGGGCACCC
Ifnb F	TCTCCACCACAGCCCTCTCC
Ifnb R	TCCGCCCTGTAGGTGAGGTT
Ifnb P	TCCATTCAGCTGCTCCAGGAGCTCCT
Ifnl2 F	AGGCCCAGAGCAAGGAGACC
Ifnl2 R	ACACTTGAGGTCCCGGGTGA
Ifnl2 P	TGGCTGCCTGGAGGCCTCTGTCACC
Ifng F	AGGTCCAGCGCCAAGCATTC
Ifng R	TCCGCTTCCTGAGGCTGGAT
Ifng P	CCGAGTGGTCCACCAGCTGTTGCCGG
Isg15 F	GTCCCAGCGGGAACAAGTCC
Isg15 R	CCCTCAGGCGCAAATGCTTG
Isg15 P	TGGGCCTTCCCTCGAAGCTCAGCCAGA
Ifit1 F	TGGGCCTTGCTGAAGTGTGG
Ifit1 R	TGGCGATAGGCTACGACTGC
Ifit1 P	AGCCATGGCCTGCTTTGCGAAGGCTCT
Mx1 F	TGGTGGACAGAGGTGCTGAA
Mx1 R	CCTGCTGACCTCTGCACTTG
Mx1 P	ACCAGGTTCCGCATCACATCCAAGAC
Oas1 F	GACTGGCGGCGTCTAGCAG
Oas1 R	GCACCTCCCAGGAGCACAC
Oas1 P	AGGCTGCCACCTGGCTGCAATACCCA
Il1b F	GGCCTTGGGCCTCAAAGGAA
Il1b R	TGCTTGGGATCCACACTCTCCA
Il1b P	TGAAAGACGGCACACCCACCCTGCAGC
Il6 F	TCCATCCAGTTGCCTTCTTGGG
Il6 R	GCCTCCGACTTGTGAAGTGGT
Il6 P	TGCTGGTGACAACCACGGCCTTCCCT
Tnfa F	GAGCAGCTGGAGTGGCTGAG
Tnfa R	GTACAACCCATCGGCTGGCA
Tnfa P	CGCGCCAACGCCCTCCTGGC
Hprt F	AAATGGTTAAGGTTGCAAG
Hprt R	CCTGAAGTACTCATTATAGTCAAGGG
Hprt P	ACTTTGTTGGATTTGAAATTCCAGACAAGTTTG

Supplementary Table 2: Semiquantitative scores assigned by a board-certified veterinary pathologist following histopathologic examination of H&Es (a) and immunohistochemical labeling for influenza A virus NP (b) of the lungs, brains, and nasal turbinates.

a.

	Bovine H5N1 10^2								Bovine H5N1 10^4							
	3dpi		5dpi		3dpi		5dpi		3dpi		5dpi		3dpi		5dpi	
	M1	M2	M3	M4	M5	M6	M7	M8	M9	M10	M11	M12	M13	M14	M15	M16
Tissue Distribution (focal=1, multifocal=2, regionally extensive=3, difuse=4)	0	0	0	0	0	0	0	0	2	2	2	1	2	2	3	3
Tracheitis	0	0	0	0	0	0	0	0	3	0	0	0	0	0	0	0
Bronchiolitis	0	0	0	0	0	0	0	0	3	3	3	2	3	3	3	3
Interstitial pneumonia	0	0	0	0	0	0	0	0	1	1	0	0	2	1	1	0
Cellular exudate	0	0	0	0	0	0	0	0	1	2	3	1	2	3	3	2
Type II pneumocyte hyperplasia	0	0	0	0	0	0	0	0	0	0	0	0	0	0	0	0
Pulmonary edema	0	0	0	0	0	0	0	0	1	1	1	0	1	1	2	0
Total Lung	**0**	**0**	**0**	**0**	**0**	**0**	**0**	**0**	**11**	**9**	**9**	**4**	**10**	**10**	**12**	**8**
Brain - Lymphoplasmacytic meningitis	0	0	0	0	0	0	0	0	0	0	0	0	0	0	0	0
Brain - Encephalitis, lymphoplasmacytic with gliosis	0	0	0	0	0	0	0	0	0	0	1	0	0	0	0	0
Brain - Malacia	0	0	0	0	0	0	0	0	0	0	0	0	0	0	0	0
Brain - Vasculitis, fibrin thrombi	0	0	0	0	0	0	0	0	0	0	0	0	0	0	0	0
Brain - Hemorrhage	0	0	0	0	0	0	0	0	0	0	1	0	0	0	0	0
Total Brain	**0**	**0**	**0**	**0**	**0**	**0**	**0**	**0**	**0**	**0**	**2**	**0**	**0**	**0**	**0**	**0**
Nasal turbinates - lymphoplasmaytic rhinitis	0	0	0	0	0	0	0	0	0	0	1	1	0	0	0	0
Nasal turbinates - ulcerations/erosions	0	0	0	0	0	0	0	0	0	0	0	0	0	0	0	0
Total Nasal turbinates	**0**	**0**	**0**	**0**	**0**	**0**	**0**	**0**	**0**	**0**	**1**	**1**	**0**	**0**	**0**	**0**

	Vietnam H5N1 10^2										Vietnam H5N1 10^4						Control			
	3dpi		6dpi		3dpi		6dpi		3dpi		6dpi		3dpi		6dpi		3dpi			
	M17	M18	M19	M20	M21	M22	M23	M24	M25	M26	M27	M28	M29	M30	M31	M32	M33	M34	M35	M36
Tissue Distribution (focal=1, multifocal=2, regionally extensive=3, difuse=4)	0	0	1	2	0	0	0	2	2	2	2	2	2	2	2	2	0	0	0	0
Tracheitis	0	0	0	1	0	0	0	0	0	0	0	0	0	0	0	0	0	0	0	0
Bronchiolitis	0	0	0	3	0	0	0	3	3	2	2	3	1	1	2	1	0	0	0	0
Interstitial pneumonia	0	0	1	0	0	0	0	1	1	1	1	1	1	0	1	1	0	0	0	0
Cellular exudate	1	0	0	3	0	0	0	2	0	1	1	0	0	0	1	0	0	0	0	0
Type II pneumocyte hyperplasia	0	0	0	0	0	0	0	0	0	0	0	0	0	0	0	0	0	0	0	0
Pulmonary edema	0	0	0	2	0	0	0	1	0	0	1	1	1	1	1	1	0	0	0	0
Total Lung	**1**	**0**	**2**	**11**	**0**	**0**	**0**	**9**	**6**	**6**	**7**	**7**	**5**	**4**	**7**	**5**	**0**	**0**	**0**	**0**
Brain - Lymphoplasmacytic meningitis	0	0	0	0	0	0	0	0	0	0	0	0	0	0	0	0	0	0	0	0
Brain - Encephalitis, lymphoplasmacytic with gliosis	0	0	0	0	0	0	0	0	0	0	0	0	0	0	0	0	0	0	0	0
Brain - Malacia	0	0	0	0	0	0	0	0	0	0	0	0	0	0	0	0	0	0	0	0
Brain - Vasculitis, fibrin thrombi	0	0	0	0	0	0	0	0	0	0	0	0	0	0	0	0	0	0	0	0
Brain - Hemorrhage	0	0	0	0	0	0	0	0	0	0	0	0	0	0	0	0	0	0	0	0
Total Brain	**0**	**0**	**0**	**0**	**0**	**0**	**0**	**0**	**0**	**0**	**0**	**0**	**0**	**0**	**0**	**0**	**0**	**0**	**0**	**0**
Nasal turbinates - lymphoplasmaytic rhinitis	0	0	0	0	0	0	0	0	0	0	0	0	0	0	0	0	0	0	0	0
Nasal turbinates - ulcerations/erosions	0	0	0	0	0	0	0	0	0	0	0	0	0	0	0	0	0	0	0	0
Total Nasal turbinates	**0**	**0**	**0**	**0**	**0**	**0**	**0**	**0**	**0**	**0**	**0**	**0**	**0**	**0**	**0**	**0**	**0**	**0**	**0**	**0**

b.

	Bovine H5N1 10^2								Bovine H5N1 10^4							
	3dpi		5dpi		3dpi		5dpi		3dpi		5dpi		3dpi		5dpi	
	M1	M2	M3	M4	M5	M6	M7	M8	M9	M10	M11	M12	M13	M14	M15	M16
Brain	0	0	0	0	0	1	0	4	1	0	4	4	0	0	3	4
Nasal turbinate	0	0	0	0	0	0	0	4	2	1	3	3	1	1	2	3
Lung	0	0	0	0	1	2	0	4	2	2	4	4	2	2	4	4

	Vietnam H5N1 10^2										Vietnam H5N1 10^4						Control			
	3dpi		6dpi		3dpi		6dpi		3dpi		6dpi		3dpi		6dpi		3dpi			
	M17	M18	M19	M20	M21	M22	M23	M24	M25	M26	M27	M28	M29	M30	M31	M32	M33	M34	M35	M36
Brain	0	0	0	0	0	0	0	0	0	0	0	1	0	0	0	0	0	0	0	0
Nasal turbinate	0	0	0	0	0	0	0	0	0	1	1	0	0	0	0	0	0	0	0	0
Lung	0	0	0	0	2	0	0	2	2	3	3	3	2	2	3	3	0	0	0	0

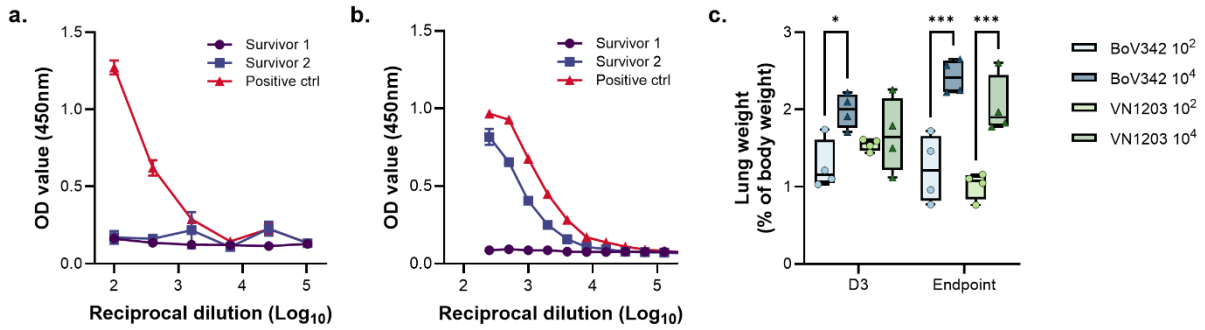

Supplementary Figure 1. a. Binding antibody titers to HA of VN1203 of two mice that survived VN1203 challenge compared to positive control mouse sera. b. Binding antibody titers to NA of A/bald eagle/Florida/W22-134-OP/2022 of two mice that survived VN1203 challenge compared to positive control NHP sera. c. Lung body weight ratio of animals inoculated with Bov342 or VN1203. Statistical significance was determined via an ordinary two-way ANOVA followed by Tukey's multiple comparisons test. * = p-value <0.05; *** = p-value <0.001.

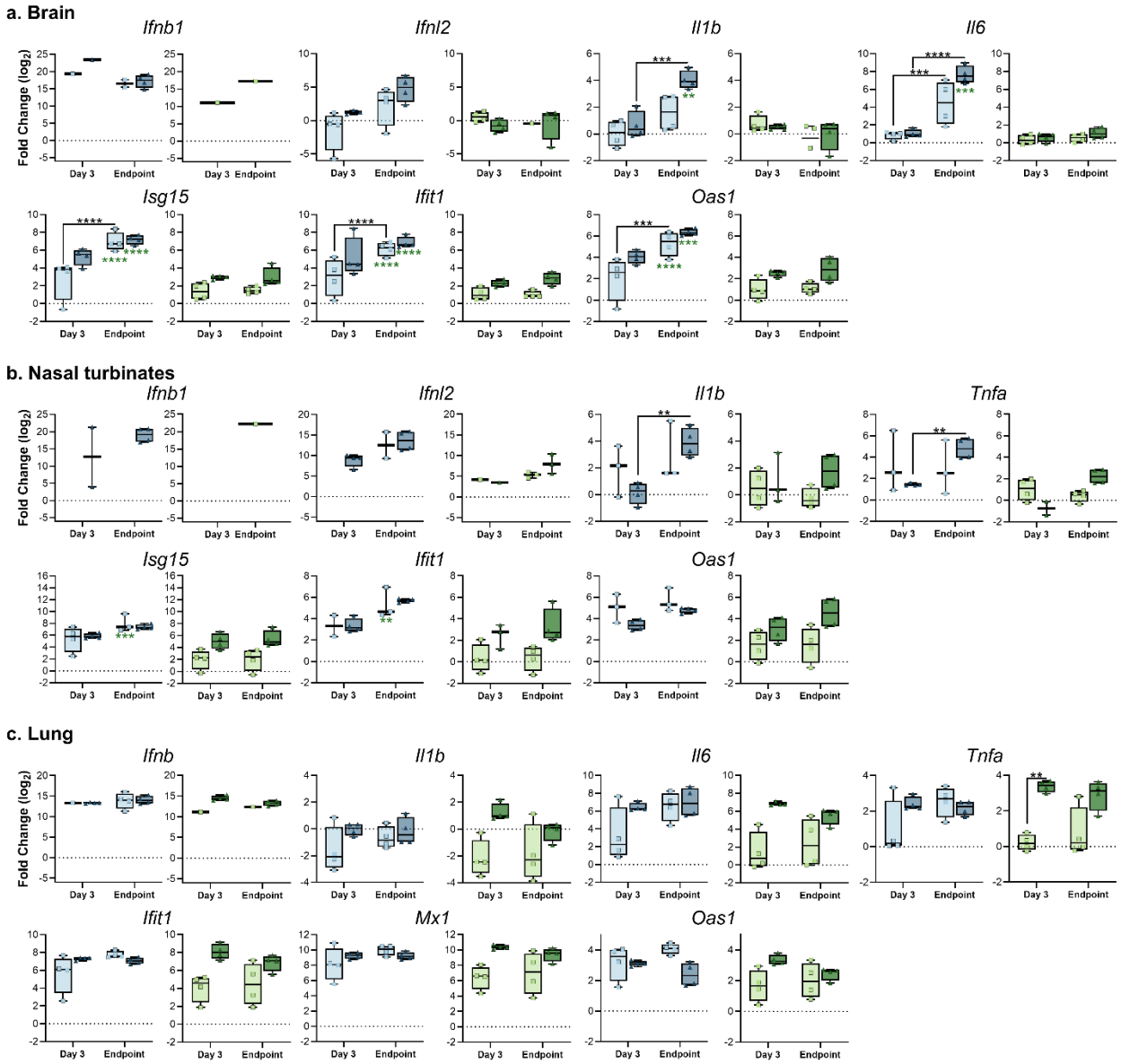

Supplementary Figure 2. Aerosol inoculation of C57Bl/6 mice with H5N1 results in virus-, tissue- and dose-dependent induction of cytokines and antiviral effector genes. Gene expression in brain (a), nasal turbinate (b), or lung (c) shown as $\log_2$ transformed fold change relative to healthy control mice. Individual values showed, bar graph shows minimum to maximum, with middle line displaying median (N=4). For genes with cycle threshold values below the limit of detection, no value is reported. Gene expression differences between viruses and dose were compared at day 3 and endpoint using a two-way ANOVA with Tukey's post-test, and differences across time points were assess with a two-way ANOVA with Sidak's multiple comparisons test. A Bonferroni correction was applied, and only p-values greater than 0.0044 were considered significant. **= p-value <0.0044, ***= p-value <0.001, ****=p-value <0.0001.

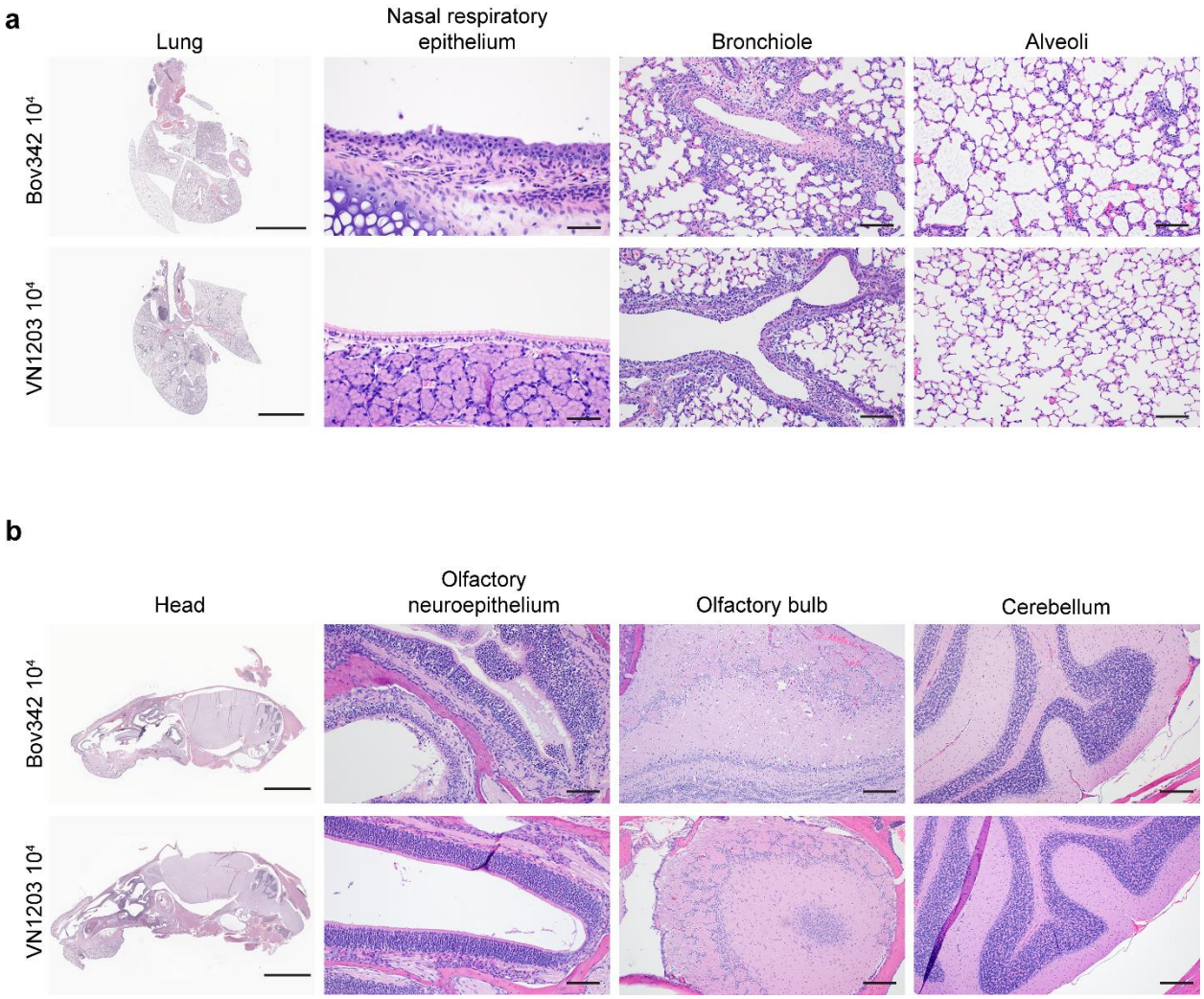

Supplementary Figure 3. **Aerosol inoculation of C57BL/6J mice with 10^4 TCID50 of both Bov342 and VN1203 result in necrotizing bronchiolitis, and no observable pathology in the CNS.** Hematoxylin and eosin (H&E) staining of lungs (a) and head (b). In the lungs, the primary histopathologic finding was a necrotizing bronchiolitis (a). Minimal pathology was observed in the nasal respiratory epithelium, and an occasional interstitial pneumonia was observed surrounding affected bronchioles (a). Significant pathology was not observed in the olfactory neuroepithelium or CNS in either Bov342 or VN1203 groups. All images were selected from representative animals in the endpoint groups. a. Lung: scale bar=4mm. Nasal respiratory epithelium: scale bar=50µm. Bronchiole: scale bar=100µm. Alveoli: scale bar=100µm. b. Head: scale bar=5mm. Olfactory neuroepithelium: scale bar=100µm. Olfactory bulb: scale bar=200µm. Cerebellum: scale bar=200 µm.

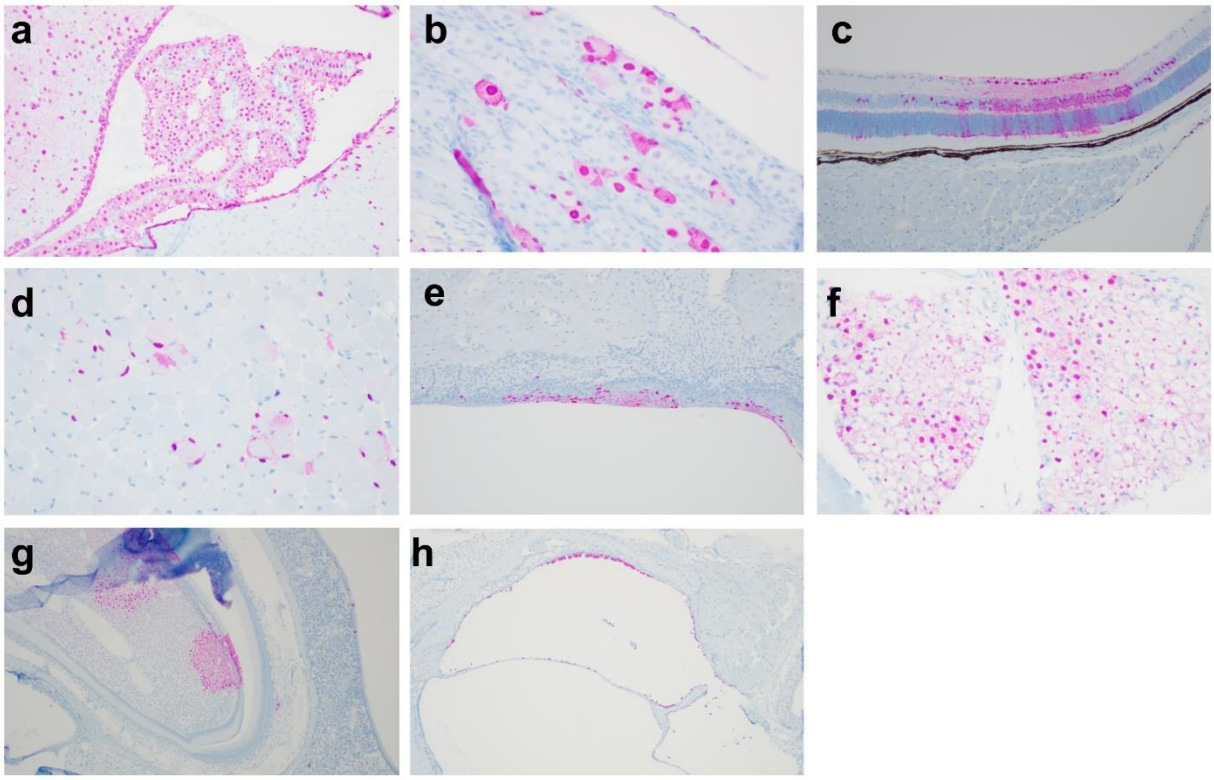

Supplementary Figure 4. Immunoreactivity for Influenza A NP was observed in multiple atypical sites within the head. IAV NP immunoreactivity (pink) was observed within the choroid plexus and ependymal cells lining the ventricle (a), large neuronal cells composing a nuclei likely associated with a cranial nerve (b), multiple cell layers of the retina (c), skeletal myocytes (d), mucosal epithelium overlying the hard palate (e), within brown adipocytes (f), within a tooth root and the overlying odontoblasts (g), and epithelial cells lining the inner ear (h).

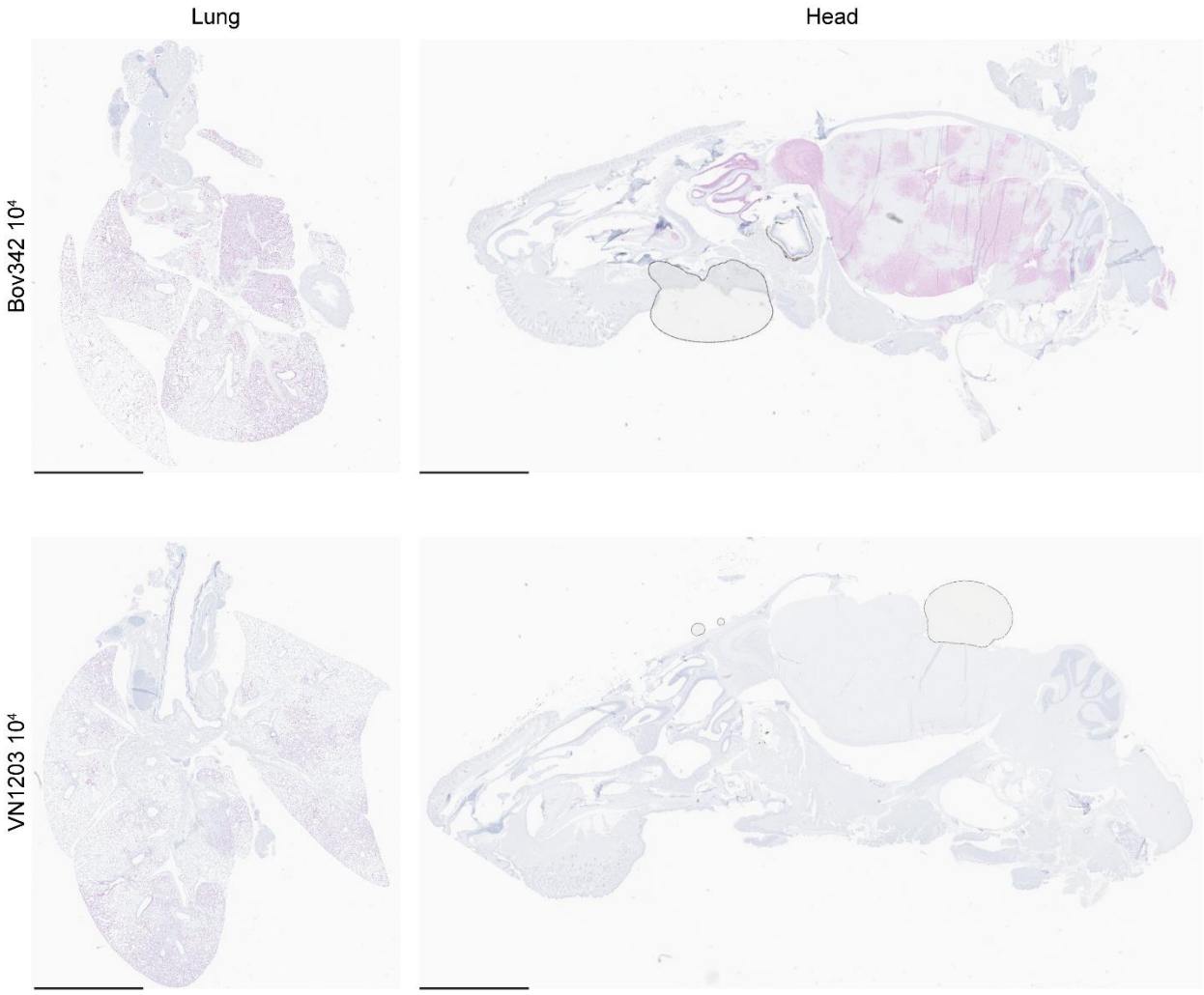

Supplementary Figure 5. Subgross photomicrographs of lung and head, immunohistochemically labeled with Influenza A NP (pink) from animals in the endpoint groups for both isolates. Immunoreactivity was observed in the lungs of both Bov342 and VN1203 animals, however IAV NP labeling was only observed in the CNS of the Bov342 animals. Representative images selected from animals in the endpoint groups for both isolates. Lung: scale bar=4mm. Head: scale bar=5mm.